Journal of Molecular Modeling (2019) 25:193
https://doi.org/10.1007/s00894-019-4064-x

ORIGINAL PAPER

Structure-based exploration of an allosteric binding pocket in the NTS1 receptor using bitopic NT(8-13) derivatives and molecular dynamics simulations

Ralf Christian Kling[1,2] · Carolin Burchardt[1] · Jürgen Einsiedel[1] · Harald Hübner[1] · Peter Gmeiner[1]

Received: 26 February 2019 / Accepted: 14 May 2019

Abstract

Crystal structures of neurotensin receptor subtype 1 (NTS1) allowed us to visualize the binding mode of the endogenous peptide hormone neurotensin and its pharmacologically active C-terminal fragment NT(8-13) within the orthosteric binding pocket of NTS1. Beneath the orthosteric binding pocket, we detected a cavity that exhibits different sequences in the neurotensin receptor subtypes NTS1 and NTS2. In this study, we explored this allosteric binding pocket using bitopic test peptides of type NT(8-13)-Xaa, in which the C-terminal part of NT(8-13) is connected to different amino acids that extend into the newly discovered pocket. Our test compounds showed nanomolar affinities for NTS1, a measurable increase in subtype selectivity compared to the parent peptide NT(8-13), and the capacity to activate the receptor in an IP accumulation assay. Computational investigation of the selected test compounds at NTS1 showed a conserved binding mode within the orthosteric binding pocket, whereas the allosteric cavity was able to adapt to different residues, which suggests a high degree of structural plasticity within that cavity of NTS1.

Keywords Structure-based drug design · Allosteric binding pocket · Neurotensin receptor · GPCR ligands · Peptide · Subtype selectivity · Molecular dynamics simulations · SPPS

Introduction

The tridecapeptide hormone neurotensin (pGlu-Leu-Tyr-Glu-Asn-Lys-Pro-Arg-Arg-Pro-Tyr-Ile-Leu-OH [1]) is known to transmit signals mainly via the G-protein-coupled receptor (GPCR) subtypes neurotensin receptor 1 (NTS1) and neurotensin receptor 2 (NTS2). NTS1 is involved in the modulation of dopaminergic signal transduction [2–4], whereas the NTS2 subtype is linked to the mediation of antinociceptive effects [5, 6]. To influence a specific receptor-mediated effect, subtype-selective ligands are necessary.

In recent years, several highly potent and subtype-selective neurotensin receptor ligands have been reported [7–15]. The majority of these compounds are likely to target the orthosteric binding pocket, a receptor domain that typically shows a high degree of sequence conservation between different receptor subtypes.

An attractive strategy for enhancing subtype selectivity is to address one or multiple topographically distinct receptor domains, which are known as allosteric or extended binding sites. These domains usually show less sequence conservation and are therefore likely to facilitate the development of subtype-selective compounds [16].

Allosteric receptor domains can be located anywhere on the GPCR, such as above the orthosteric binding site, as described for the muscarinic receptor M_2 [17], or beneath it, as observed for the chemokine receptors CCR5 [18] and CXCR4 [19]. In agreement with the latter observation, crystal structures of the NTS1 receptor [20, 21] allowed us to detect a cavity beneath and adjacent to the C-terminal end of NT(8-13) that leads to the presence of an allosteric binding site at NTS1 (Fig. 1a). Additionally, we observed a difference in

This paper belongs to the Topical Collection Tim Clark 70th Birthday Festschrift

Electronic supplementary material The online version of this article (https://doi.org/10.1007/s00894-019-4064-x) contains supplementary material, which is available to authorized users.

✉ Peter Gmeiner
peter.gmeiner@fau.de

[1] Department of Chemistry and Pharmacy, Friedrich Alexander University, Nikolaus-Fiebiger-Straße 10, 91058 Erlangen, Germany

[2] Present address: ABF-Pharmazie GmbH, Nürnberger Straße 22, 90762 Fürth, Germany

Published online: 17 June 2019

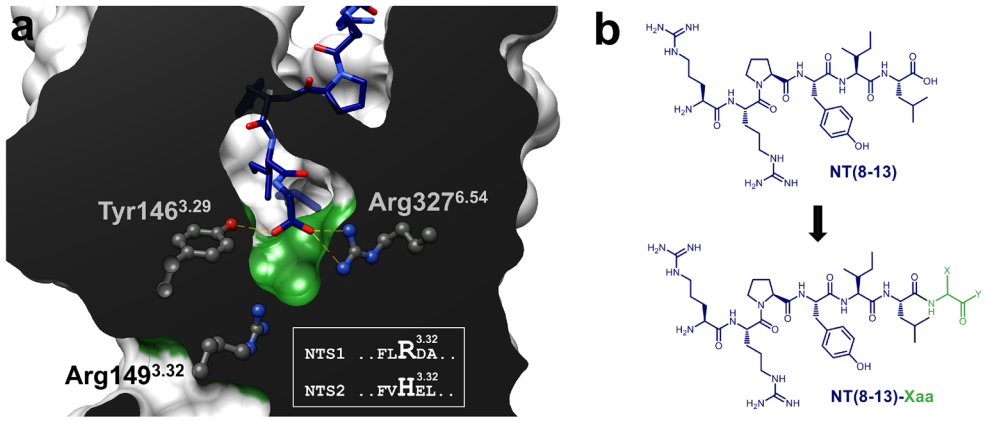

Fig. 1 Extended binding pocket of NTS1 and the general structure of compounds of type NT(8-13)-Xaa that target this pocket. **a** Close-up of the crystal structure of the NTS1 receptor coupled to NT(8-13) (PDB-ID: 4GRV), showing an extended cavity below the orthosteric binding pocket of NT(8-13) (*green surface*), which exhibits a difference in sequence from NTS2 at position 3.32 (*inset*). The carboxy-terminal end of NT(8-13) is stabilized by Arg327$^{6.54}$ and Tyr146$^{3.29}$. **b** The general chemical structure of compounds of type NT(8-13)-Xaa, which are designed to bind to the extended cavity

sequence within the binding domain between NTS1 and NTS2 (Arg149$^{3.32}$ and His115$^{3.32}$, respectively, Fig. 1a/insert), which may enable the design of subtype-selective compounds.

To explore this allosteric receptor domain as a potential new binding pocket, we used a combined approach involving chemical synthesis, biological evaluation, and molecular modeling. Encouraged by recent SAR investigations [12], we herein present the synthesis of bitopic ligands of type NT(8-13)-Xaa (Fig. 1b), which contain the NT(8-13) fragment that binds in the orthosteric pocket and an extension at the C-terminus that recognizes the allosteric site.

Starting from NT(8-13)-glycine-OH (**1a**), amino acids bearing various side chains and C-termini were synthesized and tested for their abilities to bind to NTS1 and NTS2, respectively. Selected peptides were also tested in an inositol phosphate (IP) accumulation assay to investigate their activation profiles/intrinsic activities at the NTS1 subtype. To learn more about the possible binding modes of our bitopic ligands within the allosteric cavity of human NTS1, we investigated representative test compounds using a combination of homology modeling and molecular dynamics simulations.

Methods

Chemical synthesis

The synthesis of C-terminally extended NT(8-13) derivatives of type NT(8-13)-Xaa involved microwave-assisted solid-phase supported peptide synthesis (Scheme 1).

In detail, solid-phase-supported peptide synthesis (SPPS) of the C-terminal D-alanine and L- and D-serine carboxylic acid derivatives **2b**, **3a**, and **3b**, respectively, was carried out starting from commercially available Wang resin preloaded with Fmoc-protected D-alanine and L- and D-serine, respectively. For the synthesis of the peptide carboxylic acids **7c**, **7f**, and **7g**, Wang resin was loaded with Fmoc-hTyr-OH (Fmoc-homotyrosine, leading to **7c**), Fmoc-2,6-dimethyl-Tyr-OH (leading to **7f**), or Fmoc-metaTyr-OH (Fmoc-3-hydroxy-Phe-OH, leading to **7g**) using EDC × HCl in the presence of DMAP as a catalyst. In order to obtain the peptide carboxylic acids **1a**, **2a**, **2b**, **4a**, **4b**, **5a**, **5b**, **7a**, **7b**, **7d**, **7e**, **8a–f**, and **9a–c**, 2-chlorotrityl chloride resin was loaded with Fmoc-Gly-OH (**1a**, **8a–f**, **9a–c**), Fmoc-Ala-OH (**2a**), Fmoc-Phe-OH (**4a**), Fmoc-D-Phe-OH (**4b**), *N*-Fmoc-(*S*)-3-(pyrazolo[1,5-*a*]pyridin-5-yl)-propionic acid (**5a**) *N*-Fmoc-(*S*)-3-(pyrazolo[1,5-*a*]pyridin-6-yl)-propionic acid (**5b**), Fmoc-Tyr(O^{t}Bu)-OH (**6**, **7a**, **7b**), Fmoc-*N*-MeTyr(O^{t}Bu)-OH (**7d**), or Fmoc-*N*-hTyr(O^{t}Bu)-OH (the corresponding peptoid of homotyrosine, leading to **7e**) in the presence of DIPEA. Synthesis of the C-terminal hydroxamic acid derivatives **1c** and **3d** was performed starting from 2-chlorotrityl chloride resin, which was loaded with Fmoc-protected hydroxylamine in the presence of DIPEA, with HATU/HOAt/DIPEA included to couple the next amino acid. Synthesis of the glycinol derivative **1d** was accomplished by attaching *N*-Fmoc-2-aminoethanol to 2-chlorotrityl chloride resin at 60 °C, using pyridine as the base. In all cases, residual 2-chlorotrityl chloride groups were quenched by methanol/DIPEA treatment after loading the resin. Fmoc-Rink amide AM resin was employed to synthesize the C-terminal peptide carboxamides **1b**, **2c**, and **3c**. Microwave irradiation was used to accelerate both Fmoc deprotection with piperidine and the peptide coupling of the amino acids with PyBOP, HOBt, and DIPEA. Cleavage from the resin with TFA/phenol/water/triisopropylsilane and preparative HPLC furnished the test peptides with a purity of > 95%. For further details, see Supporting Information S1 in the "Electronic supplementary material" (ESM).

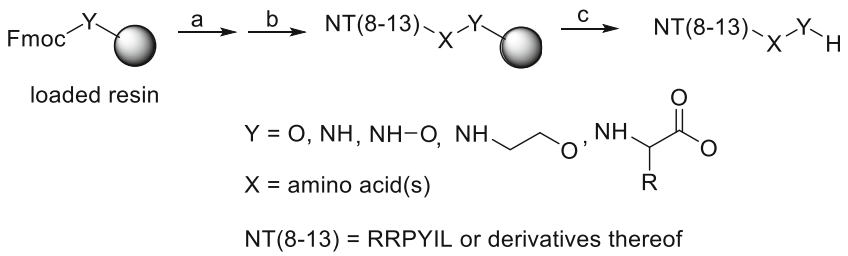

Scheme 1 Synthesis of the C-terminally extended NT(8-13)-Xaa derivatives. Reagents and conditions: *a* piperidine/DMF, microwaves; *b* Fmoc-AA-OH, PyBOP, DIPEA, HOBt, DMF, and microwaves, except in the coupling of Fmoc-Leu-OH in peptide **7f** (BTC, 2,6-lutidine, dioxane, microwaves, then rt for 2 h) and in the coupling of Fmoc Gly-OH (**1c**) and Fmoc-Ser(*t*-Bu)-OH (**3d**; Fmoc-AA/HATU/HOAt/DIPEA rt, 12 h). *c* TFA/phenol/H_2O/TIS, rt, 3 h

Receptor binding experiments

Receptor binding data were determined according to previously described protocols [8, 22]. In detail, NTS1 binding was measured using homogenates of membranes from CHO cells that stably expressed human NTS1 at a final concentration of 2 μg/well and the radioligand [^{3}H]neurotensin (specific activity 116 Ci/mmol; PerkinElmer, Rodgau, Germany) at a concentration of 0.50 nM, incubating for 60 min at 37 °C. The specific binding of the radioligand was determined at a K_D value of 0.39 ± 0.02 nM and a B_{max} value of 3600 ± 950 fmol/mg protein. Nonspecific binding was determined in the presence of 10 μM neurotensin. NTS2 binding was explored using homogenates of membranes from HEK 293, which were transiently transfected with the pcDNA3.1 vector containing the human NTS2 gene (Missouri S&T cDNA Resource Center (UMR), Rolla, MO, USA) by the calcium phosphate method [23]. The membranes were incubated for 60 min at 37 °C and a final concentration of 10–20 μg/well together with 0.50 nM [^{3}H]NT(8-13) (specific activity 136 Ci/mmol; custom synthesis of [leucine-^{3}H]NT(8-13) by GE Healthcare, Freiburg, Germany) at a K_D value of 1.2 ± 0.092 nM and a B_{max} value of 800 ± 160 fmol/mg protein. Nonspecific binding was determined in the presence of 10 μM NT(8-13), and the protein concentration was generally determined by Lowry's method using bovine serum albumin as standard [24].

The competition curves from the radioligand binding experiments were subjected to nonlinear regression analysis using algorithms in PRISM 6.0 (GraphPad Software, San Diego, CA, USA). EC_{50} values derived from the resulting dose–response curves were transformed into the corresponding K_i values utilizing the equation of Cheng and Prusoff [25].

IP accumulation

NTS1-mediated IP accumulation by the selected test compounds **1a**, **3a**, **4a**, **6**, **7c**, and **7g** as well as the reference NT(8-13) was determined using the IP-One HTRF assay (Cisbio, Codolet, France) as described previously [26]. In brief, HEK-293 cells were transiently transfected with human NTS1 (cDNA Rescourse Center, Bloomsberg, PA, USA) by applying the Mirus TransIT-293 transfection reagent (Peqlab, Erlangen, Germany). After seeding the cells into black 384-well plates (10000 cells/well) (Greiner Bio-One, Frickenhausen, Germany) and maintaining them for 24 h at 37 °C, agonist properties were determined by adding test compounds (at concentrations ranging from 0.001 nM to 10 μM) in duplicate for 90 min at 37 °C. Incubation was stopped by adding detection reagents (IP1-d2 conjugate and anti-IP1 cryptate TB conjugate, each dissolved in lysis buffer) for a further 60 min at room temperature. Time-resolved fluorescence resonance energy transfer (HTRF) was determined using a Clariostar plate reader (BMG, Ortenberg, Germany).

The agonist properties of the elongated NT(8-13)-Ser-OH derivatives **8a–f** were investigated using inositol phosphate (IP) accumulation assays, as described previously [17, 27]. [^{3}H]inositol monophosphate ([^{3}H]IP_1) was determined with CHO cells that stably expressed human NTS1. After adding *myo*-[^{3}H]inositol (specific activity = 22.5 Ci mmol^{-1}, PerkinElmer) and incubating for 15 h, the medium was aspirated, and the cells were washed with serum-free medium supplemented with 10 mM LiCl and incubated with test compounds (at concentrations ranging from 0.1 nM up to 10 μM) in triplicate for 60 min at 37 °C. After cell lysis, [^{3}H]IP_1 was separated using an AG1-X8 resin (Bio-Rad, Munich, Germany). Radioactivity was determined by scintillation counting using a Beckman (Krefeld, Germany) LS 6500.

Data analysis of the IP accumulation experiments was performed by nonlinear regression using the algorithms for log(agonist) vs. response of PRISM 6.0 (GraphPad, San Diego, CA, USA) and normalizing the raw data to the basal level (0%) and the maximum effect of NT(8-13) (100%).

Computational chemistry

To obtain initial conformations for the test compounds **1a**, **3a**, and **4a** to use in MD simulations, we used the crystal structure of rat NTS1 coupled to NT(8-13) (PDB-ID: 4GRV) [21] as a template to create a homology model of human NTS1, which

was coupled to the respective C-terminally extended compound. The program MODELLER 9v4 [28] was used according to a procedure that was successfully applied in a previous work [7], We created 100 models of each ligand–receptor complex, which mainly showed conformational differences at the C-terminally extended residues. We manually selected three representative conformations of the test compound **1a** at NTS1 (models 1–3) that (1) showed a comparable conformation to the parent peptide NT(8-13) (as indicated by our complementary experimental results) and (2) showed a different conformation of the C-terminal extension. Subsequently, models 1–3 were investigated to check the stability of their initial conformations using MD simulations. According to the conformation observed within model 1 of **1a**, we manually selected one model each of compounds **3a** and **4a** at NTS1. The ligand–receptor complexes were submitted to energy minimization using the SANDER module of AMBER10, as previously described [29]. The all-atom force field ff99SB [30] was used. Minimization was carried out as reported in the literature [7]. The AMBER parameter topology and coordinate files for the minimized complexes were converted into GROMACS [31, 32] input files and applied to a lipidic bilayer of DOPC residues as previously described [33]. The charges on the simulation systems were neutralized by adding 12 chlorine atoms each. The simulation systems were submitted to molecular dynamics simulation runs as previously described, using the GROMACS simulation package [34]. An overview of the simulation systems and their simulation times is provided in the ESM. Trajectory analysis was performed using PTRAJ of the AMBER package, and figures were prepared using PyMOL [35] and Chimera [36]. Representative conformations for compound **8d** were obtained by the homology modeling procedure described above.

Results and discussion

Our synthesis of C-terminally extended NT(8-13)-derivatives of type NT(8-13)-Xaa (Fig. 1b) involved microwave-assisted solid-phase supported peptide synthesis (SPPS), starting from chlorotrityl chloride resin, Rink amide resin, or Wang resin (preloaded with a suitable Fmoc-amino acid in some cases), which were reacted as described in the "Methods" section. A more detailed description of the syntheses and analytical data of the test compounds explored in this study is provided in Supporting Information S1 of the ESM.

Radioligand binding studies were conducted to evaluate the NTS1 and NTS2 affinities of all the synthesized compounds (Tables 1–3, Supporting Information S2 of the ESM). Binding data were determined utilizing the radioligand [^{3}H]neurotensin and Chinese hamster ovary (CHO) cells that stably expressed human NTS1. [^{3}H]NT(8-13) was used for binding assays carried out to investigate human NTS2, which was transiently transfected into human embryonic kidney (HEK 293) cells. To investigate the intrinsic activities of some of the described elongated peptides in comparison with NT(8-13), we used an inositol phosphate (IP) accumulation assay in which the $G\alpha_q$-promoted modulation of IP production in cells expressing NTS1 was recorded (Tables 1 and 2).

The obtained binding data support the existence of the postulated allosteric binding pocket below the C-terminus of bound NT(8-13), and point to interesting structure–activity relationships (SAR) for this cavity (Table 1). The K_i values of the glycine derivatives **1a**–**c**, which bear a carboxylic acid (**1a**), an amide (**1b**), or a hydroxamic acid (**1c**) as a C-terminal functional group, are all comparable for both subtypes, whereas deletion of the carbonyl group, as implemented in the alcohol **1d**, leads to a fiftyfold or fivefold loss of affinity at NTS1 or NTS2, respectively, indicating the importance of the presence of a carbonyl function in combination with a group which is able to form hydrogen bonds (but not necessarily an ionic interaction) for receptor recognition. These results are supported by data obtained for the alanine derivatives **2a** and **2c** as well as the serine derivatives **3a**, **3c**, and **3d**. With the introduction of more complex amino acids, we were able to enhance the affinity as well as the selectivity compared to our starting compound NT(8-13)-glycine **1a**. Introducing both a methyl group (**2a**) and an aromatic system (**4a**) at the Cα atom increased NTS1 affinity (1 nM and 0.9 nM, respectively), whereas the additional insertion of a hydroxyl function (**3a**) led to enhanced selectivity (> 18-fold) for NTS1 over NTS2, in combination with a good single-digit nanomolar NTS1 affinity (3.3 nM). Modifying the aromatic moiety of **4a** by inserting the recently described 5-substituted azaindolyl alanine (peptide **5**) did not result in a significant improvement. In contrast, introducing a tyrosine at this position (peptide **6**) led us to the very promising NTS1-selective compound **6**, offering NTS1 binding of 1.3 nM and a 26-fold selectivity for NTS1 over NTS2. Further modifications of the parent compound **6** that led to compounds **7a**–**7g** did not result in any further gain in affinity or selectivity (Table 1). The same is true of the insertion of other functional amino acid side chains, such as basic or acidic residues, or homologation of the backbone via the insertion of β-amino acids (see Supporting Information S2 in the ESM).

Interestingly, the addition of L-amino acids increased NTS1 selectivity compared to the parent peptide NT(8-13), whereas the addition of the corresponding D-amino acids yielded a decrease in NTS1 selectivity or even a preference for NTS2 binding (Table 1, Supporting Information S2 in the ESM).

Remarkably, all of the investigated peptides showed agonist behavior and were able to activate NTS1 at levels of 92–100% compared to NT(8-13); see Table 1.

To learn more about the possible binding modes of our bitopic ligands, we investigated representative test compounds exhibiting glycine (**1a**), serine (**3a**), or phenylalanine

Table 1 Receptor-binding data for bitopic ligands **1a–7g**[a] in comparison to the reference agent NT(8-13), and functional IP accumulation assay results for selected compounds

Compound	Peptide	K_i value[b] (nM)		Selectivity	IP accumulation assay[c]	
		NTS1[d] [^{3}H]neurotensin	NTS2[e] [^{3}H]NT(8-13)	K_i(NTS2)/ K_i(NTS1)	EC_{50} value[f]	Efficacy[g]
NT(8-13)		0.24 ± 0.048	1.2 ± 0.25[h]	5.0	0.74 ± 0.20	100%
1a	NT(8-13)-Gly-OH	6.8 ± 4.5	53 ± 21	7.8	18 ± 4	98 ± 2%
1b	NT(8-13)-Gly-NH_2	5.0 ± 2.3	36 ± 16	7.2	–	–
1c	NT(8-13)-Gly-NHOH	4.8 ± 2.4	57 ± 52	12	–	–
1d	NT(8-13)-Glycinol	270 ± 230	240 ± 170	0.9	–	–
2a	NT(8-13)-Ala-OH	1.0 ± 0.11	13 ± 4.6	13	–	–
2b	NT(8-13)-D-Ala-OH	20 ± 2.3	8.1 ± 5.7	0.4	–	–
2c	NT(8-13)-Ala-NH_2	1.9 ± 0.49	23 ± 7.7	12	–	–
3a	NT(8-13)-Ser-OH	3.3 ± 1.7	58 ± 28	18	37 ± 16	98 ± 5%
3b	NT(8-13)-D-Ser-OH	23 ± 15	44 ± 7.1	1.9	–	–
3c	NT(8-13)-Ser-NH_2	2.9 ± 1.2	25 ± 16	8.6	–	–
3d	NT(8-13)-Ser-NHOH	4.0 ± 2.9	27 ± 2.3	6.8	–	–
4a	NT(8-13)-Phe-OH	0.91 ± 0.49	12 ± 4.0	13	150 ± 22	100 ± 5%
4b	NT(8-13)-D-Phe-OH	210 ± 89	360 ± 250	1.7	–	–
5a	NT(8-13)-5-PP-OH	2.6 ± 0.20	25 ± 19	9.6	–	–
5b	NT(8-13)-6-PP-OH	6.9 ± 4.1	32 ± 21	4.6	–	–
6	NT(8-13)-Tyr-OH	1.3 ± 0.38	34 ± 9.4	26	110 ± 26	95 ± 10%
7a	[*N*-MeArg^8]-NT(8-13)-Tyr-OH	1.2 ± 0.68	16 ± 3.1	13	–	–
7b	[D-Arg^8]-NT(8-13)-Tyr-OH	3.7 ± 2.6	73 ± 48	20	–	–
7c	NT(8-13)-hTyr-OH	1.5 ± 0.65	37 ± 9.1	25	24 ± 5	92 ± 8%
7d	NT(8-13)-*N*-MeTyr-OH	150 ± 110	3400 ± 2400	23	–	–
7e	NT(8-13)-*N*-hTyr-OH	700 ± 160	11000 ± 4600	16	–	–
7f	NT(8-13)-Dmt-Tyr-OH	12 ± 3.7	120 ± 7.1	10	–	–
7g	NT(8-13)-*meta*-Tyr-OH	2.1 ± 0.4	44 ± 23	21	34 ± 7	94 ± 4%

[a] HPLC and LCMS studies were performed for representative compounds, verifying that they were stable with respect to degradation within the buffer used for the binding experiments (see Supporting Information S10 in the ESM). [b] K_i values in nM ± SD are the means of 3–9 individual experiments, each done in triplicate. [c] IP accumulation was measured using the IP-One assay (Cisbio) with HEK cells that transiently expressed human NTS1. [d] Membranes from CHO cells that stably expressed human NTS1. [e] Homogenates from HEK 293 cells transiently transfected with human NTS2. [f] EC_{50} values in nM ± SD are the means of 3–4 individual experiments, each done in duplicate. [g] Maximum effect in % ± SD relative to the full response of NT(8-13). [h] K_D value

(**4a**) as a C-terminal extension, using a combination of homology modeling and molecular dynamics (MD) simulations. We used the conformation of NT(8-13) observed within the crystal structure of rat NTS1 as a structural scaffold to which the C-terminal residue was attached in order to facilitate the generation of feasible initial conformations of **1a**, **3a**, and **4a** for subsequent MD simulation runs (see Supporting Information S3 and S4 in the ESM).

Upon comparing the final conformations of the investigated test compounds at human NTS1 (see Supporting Information S5 in the ESM), we observed, in general, well-conserved hydrogen-bond interactions that stabilized the orthosteric parts of our test compounds, most of which were localized within the aforementioned crystal structure (see Supporting Information S6 in the ESM). Thus, the C-terminal extensions of our test compounds are capable of engaging an allosteric cavity, which consists of residues from TM2, TM3, TM6, and TM7 (Fig. 2a, Supporting Information S6 in the ESM) and is located directly below the orthosteric binding pocket, when the specific additional interactions between the elongated compounds and residues of NTS1 depend on the nature of the attached residue.

Focusing on the C-terminal glycine of compound **1a**, we observed that its carboxyl moiety adopts a conformation in which it is not only able to form a stable interaction with residue Arg149$^{3.32}$ in the allosteric cavity of NTS1 (as intended) but is also able to form interactions with residues Arg322$^{6.54}$ and Arg323$^{6.55}$ (Fig. 2b, c). The three arginine residues are part of a structurally distinct hydrogen bond/ionic interaction network that is structurally bridged by the specific spatial arrangement of the carboxyl group of compound **1a** (see Supporting Information S7 in the ESM).

Table 2 Receptor binding data for the C-terminally extended NT(8-13)-derivatives **8a–8f**[a] in comparison to the reference agent NT(8-13), and results of the functional IP accumulation assay

Compound	Peptide	K_i value[b] (nM)		Selectivity	IP accumulation assay[c]	
		NTS1[d] [^{3}H]neurotensin	NTS2[e] [^{3}H]NT(8-13)	K_i(NTS2)/ K_i(NTS1)	EC_{50} value[f]	Efficacy[g]
NT(8-13)		0.24 ± 0.048	1.2 ± 0.25[h]	5.0	0.34 ± 0.14	100%
8a	NT(8-13)-Ser-Gly-OH	3.1 ± 1.9	15 ± 8.5	4.8	13 ± 12	102 ± 11%
8b	NT(8-13)-Ser-Gly_2-OH	2.0 ± 1.4	7.9 ± 3.4	4.0	13 ± 2	99 ± 8%
8c	NT(8-13)-Ser-Gly_3-OH	8.8 ±3.4	28 ± 8.7	3.2	–	–
8d	NT(8-13)-Ser-Gly_4-OH	11 ± 6.2	33 ± 14	3.0	125 ± 78	108 ± 7%
8e	NT(8-13)-Ser-Gly_7-OH	24 ± 14	50 ± 14	2.1	180 ± 39	87 ± 14%
8f	NT(8-13)-Ser-Gly_9-OH	23 ± 7.4	200 ± 39	8.7	1100 ± 420	106 ± 1%

[a] HPLC and LCMS studies were performed for representative compounds, verifying that they were stable with respect to degradation within the buffer used for the binding experiments (see Supporting Information S9 in the ESM). [b] K_i values in nM ± SD are the means of 3-4 individual experiments, each done in triplicate. [c] IP accumulation was measured using a [^{3}H]inositol-based IP_1 assay with CHO cells that stably expressed human NTS1. [d] Membranes from CHO cells that stably expressed human NTS1. [e] Homogenates from HEK 293 cells transiently transfected with human NTS2. [f] EC_{50} values in nM ± SD are the means of 3-4 individual experiments, each done in triplicate. [g] Maximum effect in % ± SD relative to the full response of NT(8-13). [h] K_D value.

The insertion of certain side chains to give test compounds **3a** and **4a** resulted in slightly altered binding modes compared to **1a**, enabling the formation of specific interactions of **3a** and **4a** with residues of NTS1 (Fig. 2a). This suggests a (limited) capacity of the allosteric cavity to adapt to more sterically demanding amino acids than glycine. For the serine residue of compound **3a**, we observed a stabilization of its side chain via hydrogen bonds between its hydroxyl moiety and either its own carboxyl terminus or Tyr346$^{7.35}$ of NTS1 (Fig. 2d). In contrast, the conformation of the side chain of phenylalanine (**4a**) was found to be embedded within a hydrophobic cavity involving van der Waals interactions with Glu123$^{2.61}$, π–π interactions with Phe127$^{2.65}$, Tyr145$^{3.28}$, and Tyr146$^{3.29}$, and cation–π interactions with Arg149$^{3.32}$, whereas its carboxyl terminus formed a hydrogen bond with Tyr346$^{7.35}$ (Fig. 2e, Supporting Information S8 in the ESM). These extensive interactions appear to contrast with the rather similar affinity of the test compound **4a** to those of, for example, **1a** or **3a**. Interestingly, we detected a near-perfectly stable hydrogen-bond interaction between the side chain of Tyr11 in **4a** and the backbone carbonyl of His^{EL1}. This contrasts with the homologous side chains of **1a** and **3a**, which are alternately hydrogen bonded to the backbone carbonyl atoms of His131^{EL1} and the N-terminal residue Leu56 (see Supporting Information S6 in the ESM). Since a hydrogen bond between Tyr11 and Leu56 is missing from **4a**, Tyr11 adopts a more deeply buried conformation compared to **1a** and **3a** (Fig. 2a), thereby losing stabilizing van der Waals interactions to the N-terminal domain of NTS1, which was previously suggested to be linked to a reduced binding affinity of NT(8-13) derivatives for NTS1 [7] and may therefore compensate for the gain in binding affinity via the C-terminal interactions described above.

Although the explicit conformations of **3a** and **4a** were found to differ with respect to the elongated amino acids serine and phenylalanine, respectively, the side-chain

Table 3 Human NTS1 and NTS2 receptor binding data for the NT(8-13)-Ser-Gly_4-OH-derivatives **9a–c**[a]

Compound	Peptide	K_i value[b] (nM)		Selectivity
		NTS1[c] [^{3}H]neurotensin	NTS2[d] [^{3}H]NT(8-13)	K_i(NTS2)/ K_i(NTS1)
	[Ala^{11}]NT(8-13)-OH[[8]]	1300 ± 470	83 ± 10	0.06
	[Ala^{12}]NT(8-13)-OH[[8]]	100 ± 11	63 ± 12	0.63
9a	[Ala^{11}]NT(8-13)-Ser-Gly_4-OH	36000 ± 25000	8000 ± 2600	0.22
9b	[Ala^{12}]NT(8-13)-Ser-Gly_4-OH	9500 ± 3100	4900 ± 1100	0.52
9c	H-Arg-Arg-Pro-Ile-Leu-Ser-Gly_4-OH	>100000[e]	>100000[e]	nd

[a] HPLC and LCMS studies were performed for representative compounds, verifying that they were stable with respect to degradation within the buffer used for the binding experiments (see Supporting Information S9 in the ESM). [b] K_i values in nM ± SD are the means of 3-4 individual experiments each done in triplicate. [c] Membranes from CHO cells that stably expressed human NTS1. [d] Membranes from CHO cells that stably expressed human NTS2. [e] K_i values in nM ± SD derived from two individual experiments, each done in triplicate. *nd* could not be determined

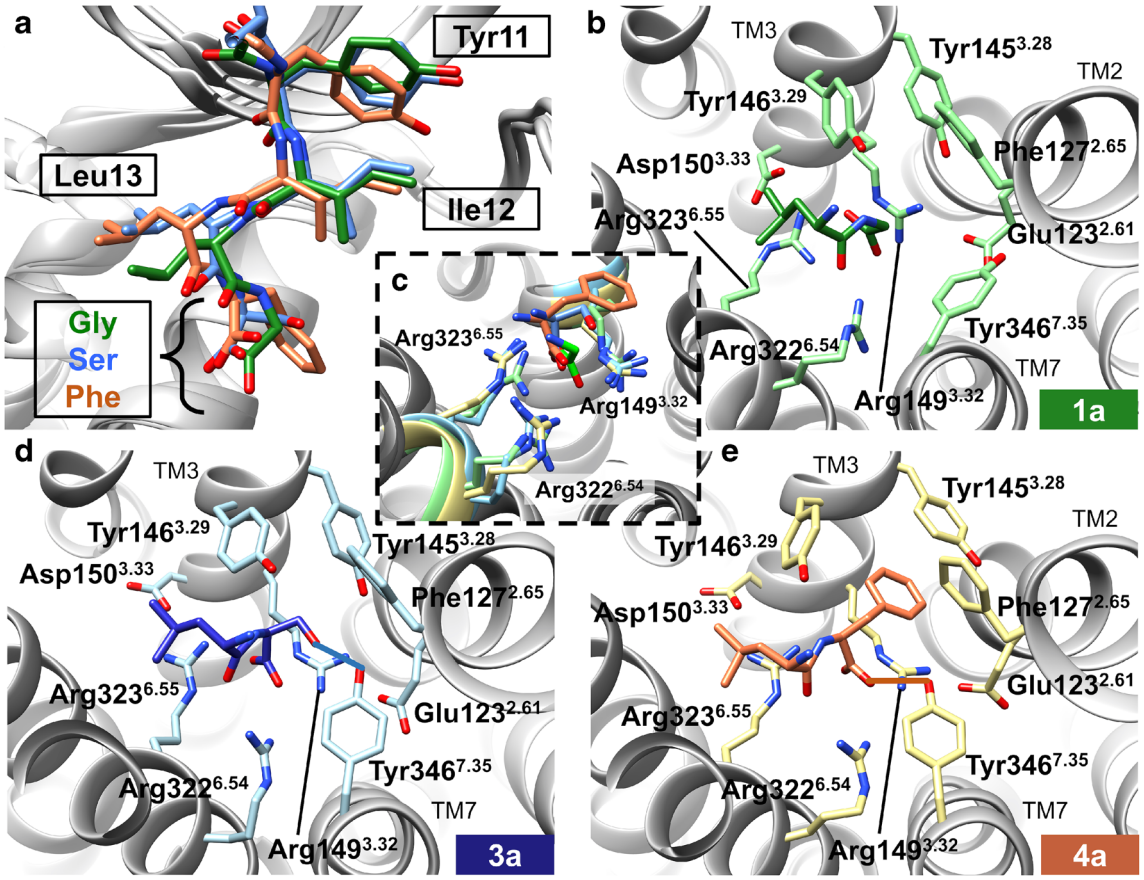

Fig. 2 Ligand–receptor interactions within the individual simulation systems. Close-ups of representative snapshots of ligand–receptor interactions within the extended binding pocket of NTS1 are shown for the individual simulation systems **1a** (**b**), **3a** (**d**), and **4a** (**e**). An overlay of representative conformations of the test compounds is provided that focuses on C-terminal residues of NT(8-13)-Xaa (**a**, **c**). The test compounds **1a**, **3a**, and **4a** are shown as *green*, *blue*, and *orange sticks*, respectively, whereas the main chain of NTS1 is shown in *gray*. Residues of NTS1 that are interacting with **1a**, **3a**, and **4a** are shown as *light green*, *light blue*, and *yellow sticks*, respectively

conformations of **3a** and **4a** enabled similar spatial arrangements of their carboxyl groups, resulting in the simultaneous formation of interactions with Arg149$^{3.32}$, Arg322$^{6.54}$, and Arg323$^{6.55}$, as already observed for compound **1a** (Fig. 2c). We thus attribute a key role to the carboxyl group in **1a**, **3a**, and **4a** in stabilizing the conformations of these bitopic compounds, implying that the presence of this group is a major determinant of the excellent binding affinities of these compounds for NTS1. As the homologous residue of Arg149$^{3.32}$ is a smaller histidine at NTS2 (His115$^{3.32}$, Fig. 1 and Supporting Information S9 in the ESM), it is tempting to assume the presence of a less well-stabilized interaction network between the allosteric cavity of NTS2 and the carboxyl group of the bitopic compounds, which may increase the entropic cost of forming C-terminal interactions, thus providing an explanation for the reduced affinities of these compounds for NTS2.

Encouraged by our results which suggested that the extended binding pocket had high structural plasticity, we aimed to investigate whether the neurotensin receptor is able to accommodate even more elongated test compounds. Thus, starting from compound **3a**, we attached up to nine glycine residues as C-terminal extensions (compounds **8a–8f**).

Surprisingly, the resulting molecular probes showed remarkable receptor binding, with K_i values in the nanomolar range (Table 2). Starting from **3a**, the addition of one (**8a**) and two (**8b**) glycine residues increased affinity to 2 nM but reduced selectivity, whereas the addition of further glycines reduced the affinity up to tenfold while slightly increasing the NTS1 selectivity. Consistent with our results, the NTS1 receptor seems to be more tolerant of such C-terminal extensions than NTS2. Again, all these compounds were able to activate NTS1 in an IP accumulation assay, although the efficacy of compound **8f** dropped disproportionately compared to its loss of affinity. Our results make it tempting to assume the presence of an even larger allosteric pocket beneath the binding pocket of NT(8-13) without altering the signaling capacity of NTS1. In our model, the Cα atom of the terminal glycine of compound **8d** would be more than 20 Å away from the extracellular surface of NTS1 and only about 15 Å away from the canonical residue Arg165$^{3.50}$ (Fig. 3). Interestingly, our model

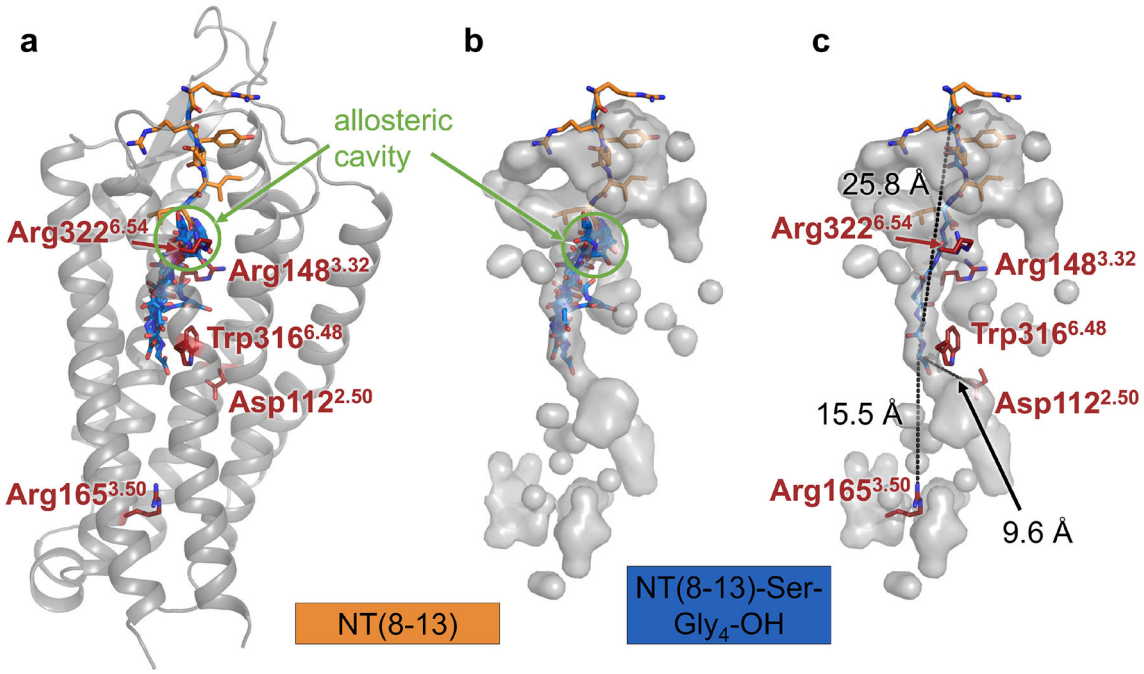

Fig. 3 Representative conformations of compound **8d** (NT(8-13)-Ser-Gly_4-OH) superimposed on the crystal structure of NTS1. **a** Side view of the crystal structure of the NTS1 receptor coupled to NT(8-13) (PDB-ID: 4GRV), showing eight representative conformations of **8d** (*blue sticks*) obtained by homology modeling. NT(8-13) and selected residues of NTS1 are visualized as *orange* and *red sticks*, respectively. **b** Superposition of the conformations of **8d** from **a** on the interior surface representation of NTS1. The C-terminal extension of **8d** forms a tube extending from the allosteric cavity (*highlighted in green*) beneath the orthosteric binding pocket of NTS1. **c** Distances between the Cα atom of the C-terminal glycine residue of **8d** and the residues Asp112$^{2.50}$ and Arg165$^{3.50}$ as well as the top of the extracellular surface of NTS1

suggests that the highly conserved residue Trp316$^{6.48}$ is involved in stabilizing the conformation of our test compound.

In this study, we assumed that our test compounds are bitopic such that their orthosteric part, i.e., NT(8-13), uses the same binding pocket as and adopts a similar conformation to unaltered NT(8-13) but the C-terminal extension makes its way into the allosteric cavity of the neurotensin receptor. This assumption is fully consistent with our computational experiments. Nevertheless, we tested this assumption by performing further experiments in which we replaced Tyr11 and Ile12 with alanine. These two residues of NT(8-13) had previously been shown to be essential to the binding of NT(8-13) [8], and were therefore changed in the NT(8-13) pharmacophore of **8d**, resulting in the test compounds **9a** and **9b**, respectively. In addition, we synthesized compound **9c**, in which Tyr11 is completely removed. If the orthosteric part of each bitopic test compound had a comparable binding mode to NT(8-13), one would expect a significant loss of affinity at the neurotensin receptor. Consistent with this hypothesis, our results show the expected loss of affinity for the test compounds **9a** and **9b** in a way that is comparable to the respective NT(8-13) derivatives (Table 3). The ΔTyr11 mutant **9c** completely loses the capacity to bind to NTS1 and NTS2.

Conclusion

Analyzing the crystal structures of the NTS1 receptor [20, 21], we detected an allosteric binding site at NTS1 beneath the C-terminus of NT(8-13). A sequence analysis revealed a difference between NTS1 and NTS2 (Arg149$^{3.32}$ and His115$^{3.32}$, respectively) within this receptor domain, which may enable the design of subtype-selective compounds. Taking advantage of these observations, we synthesized a set of new bitopic neurotensin receptor ligands of type NT(8-13)-Xaa. Subsequent binding studies of these compounds indicated that they show an encouraging tendency to bind selectively to NTS1. Upon introducing a tyrosine residue as a C-terminal extension (peptide **6**), we were able to identify a very promising NTS1-selective peptide offering NTS1 binding of 1 nM and a 26-fold selectivity for NTS1 rather than NTS2. This peptide represents a new class of neurotensin receptor ligands that simultaneously address both the orthosteric binding pocket and a newly detected allosteric binding pocket. The investigated test compounds even maintained the capacity to activate the NTS1 receptor, albeit with reduced potency compared to NT(8-13). Upon adding up to ten additional residues to the C-terminus of NT(8-13), we found that the allosteric cavity seemed to extend even further into the transmembrane region of the receptor.

To learn more about the possible binding mode of the bitopic ligands within the extended cavity in human NTS1, we investigated representative test compounds with one additional residue as a C-terminal extension using a combination of homology modeling and MD simulations (compounds **1a**, **3a**, and **4a**). We found that the test compounds investigated adopted a bitopic binding mode at human NTS1, with the NT(8-13) fragment occupying the orthosteric pocket and the amino acid extension addressing the allosteric cavity. All of the compounds investigated presented similar carboxyl group conformations and thus a set of similar interactions with residues of NTS1, whereas other interactions between the elongated compounds and residues of NTS1 (i.e., specific hydrogen bonds for **3a** or binding in a hydrophobic subpocket for **4a**) were dependent on the nature of the attached residue.

Taken together, these MD simulations were able to provide a molecular description of possible bitopic binding modes for our C-terminally extended peptides at human NTS1, which helped to characterize a newly discovered allosteric binding pocket at neurotensin receptors that exhibited remarkable structural plasticity. Although there seems to be an upper limit on the degree of subtype selectivity that can be achieved through the use of C-terminally extended peptides, the results of our study represent a promising starting point for virtual screening campaigns aimed at identifying highly NTS1-selective agonists and allosteric modulators.

References

1. Carraway R, Leeman SE (1975) The amino acid sequence of a hypothalamic peptide, neurotensin. J Biol Chem 250:1907–1911
2. Binder EB, Kinkead B, Owens MJ, Nemeroff CB (2001) Neurotensin and dopamine interactions. Pharmacol Rev 53:453–486
3. Kasckow J, Nemeroff CB (1991) The neurobiology of neurotensin: focus on neurotensin-dopamine interactions. Regul Pept 36:153–164
4. Fuxe K, Von Euler G, Agnati LF et al (1992) Intramembrane interactions between neurotensin receptors and dopamine D2 receptors as a major mechanism for the neuroleptic-like action of neurotensin. Ann New York Acad Sci 668:186–204
5. Clineschmidt BV, McGuffin JC, Bunting PB (1979) Neurotensin: antinocisponsive action in rodents. Eur J Pharmacol 54:129–139
6. Boules M, Liang Y, Briody S et al (2010) NT79: a novel neurotensin analog with selective behavioral effects. Brain Res 1308:35–46. https://doi.org/10.1016/j.brainres.2009.10.050
7. Schaab C, Kling RC, Einsiedel J et al (2014) Structure-based evolution of subtype-selective neurotensin receptor ligands. Chem Open 3:206–218. https://doi.org/10.1002/open.201402031
8. Einsiedel J, Held C, Hervet M et al (2011) Discovery of highly potent and neurotensin receptor 2 selective neurotensin mimetics. J Med Chem 54:2915–2923. https://doi.org/10.1021/jm200006c
9. Harterich S, Koschatzky S, Einsiedel J, Gmeiner P (2008) Novel insights into GPCR–peptide interactions: mutations in extracellular loop 1, ligand backbone methylations and molecular modeling of neurotensin receptor 1. Bioorg Med Chem 16:9359–9368. https://doi.org/10.1016/j.bmc.2008.08.051
10. Held C, Hübner H, Kling R et al (2013) Impact of the proline residue on ligand binding of neurotensin receptor 2 (NTS2)-selective peptide-peptoid hybrids. ChemMedChem 8:772–778. https://doi.org/10.1002/cmdc.201300054
11. Pratsch G, Unfried JF, Einsiedel J et al (2011) Radical arylation of tyrosine and its application in the synthesis of a highly selective neurotensin receptor 2 ligand. Org Biomol Chem 9:3746–3752. https://doi.org/10.1039/C1ob05292f
12. Einsiedel J, Hubner H, Hervet M et al (2008) Peptide backbone modifications on the C-terminal hexapeptide of neurotensin. Bioorg Med Chem Lett 18:2013–2018. https://doi.org/10.1016/j.bmcl.2008.01.110
13. Richelson E, McCormick DJ, Pang Y-P, Phillips KS (2009) Peptide analogs that are potent and selective for human neurotensin preceptor subtype 2. US Patent US20110263507A1
14. Cusack B, McCormick DJ, Pang YP et al (1995) Pharmacological and biochemical profiles of unique neurotensin 8-13 analogs exhibiting species selectivity, stereoselectivity, and superagonism. J Biol Chem 270:18359–18366
15. Tourwe D, Iterbeke K, Török G, et al (2002) Pro10-Tyr11 substitutions provide potent or selective NT(8-13) analogs. In: Benedetti E, Pedone C (eds) Peptides 2002, Proc 27th European Peptide Symposium, Napoli, Italy, 31 Aug–6 Sept 2002, pp 304–305
16. Valant C, Robert Lane J, Sexton PM, Christopoulos A (2012) The best of both worlds? Bitopic orthosteric/allosteric ligands of g protein-coupled receptors. Ann Rev Pharmacol Toxicol 52:153–178. https://doi.org/10.1146/annurev-pharmtox-010611-134514
17. Kruse AC, Ring AM, Manglik A et al (2013) Activation and allosteric modulation of a muscarinic acetylcholine receptor. Nature 504:101–106. https://doi.org/10.1038/nature12735
18. Tan Q, Zhu Y, Li J et al (2013) Structure of the CCR5 chemokine receptor-HIV entry inhibitor maraviroc complex. Science 341:1387–1390. https://doi.org/10.1126/science.1241475
19. Wu B, Chien EY, Mol CD et al (2010) Structures of the CXCR4 chemokine GPCR with small-molecule and cyclic peptide antagonists. Science 330:1066–1071. https://doi.org/10.1126/science.1194396
20. Egloff P, Hillenbrand M, Klenk C et al (2014) Structure of signaling-competent neurotensin receptor 1 obtained by directed evolution in *Escherichia coli*. Proc Natl Acad Sci USA 111:655–662. https://doi.org/10.1073/pnas.1317903111
21. White JF, Noinaj N, Shibata Y et al (2012) Structure of the agonist-bound neurotensin receptor. Nature 490:508–513. https://doi.org/10.1038/nature11558
22. Hubner H, Haubmann C, Utz W, Gmeiner P (2000) Conjugated enynes as nonaromatic catechol bioisosteres: synthesis, binding experiments, and computational studies of novel dopamine receptor agonists recognizing preferentially the D(3) subtype. J Med Chem 43:756–762
23. Jordan M, Schallhorn A, Wurm FM (1996) Transfecting mammalian cells: optimization of critical parameters affecting calcium-phosphate precipitate formation. Nucleic Acids Res 24:596–601
24. Lowry OH, Rosebrough NJ, Farr AL, Randall RJ (1951) Protein measurement with the Folin phenol reagent. J Biol Chem 193:265–275
25. Cheng Y, Prusoff WH (1973) Relationship between the inhibition constant (K1) and the concentration of inhibitor which causes 50 per cent inhibition (I50) of an enzymatic reaction. Biochem Pharmacol 22:3099–3108
26. Liu H, Hofmann J, Fish I et al (2018) Structure-guided development of selective M3 muscarinic acetylcholine receptor antagonists. Proc Natl Acad Sci 115:12046–12050. https://doi.org/10.1073/pnas.1813988115

27. Weichert D, Kruse AC, Manglik A et al (2014) Covalent agonists for studying G protein-coupled receptor activation. Proc Natl Acad Sci USA 111:10744–10748. https://doi.org/10.1073/pnas.1410415111
28. Šali A, Blundell TL (1993) Comparative protein modelling by satisfaction of spatial restraints. J Molec Biol 234:779–815. https://doi.org/10.1006/jmbi.1993.1626
29. Hiller C, Kling RC, Heinemann FW et al (2013) Functionally selective dopamine D2/D3 receptor agonists comprising an enyne moiety. J Med Chem 56:5130–5141. https://doi.org/10.1021/jm400520c
30. Hornak V, Abel R, Okur A et al (2006) Comparison of multiple Amber force fields and development of improved protein backbone parameters. Proteins 65:712–725. https://doi.org/10.1002/prot.21123
31. van der Spoel D, Lindahl E, Hess B et al (2005) GROMACS: fast, flexible, and free. J Comput Chem 26:1701–1718. https://doi.org/10.1002/jcc.20291
32. Hess B, Kutzner C, van der Spoel D, Lindahl E (2008) GROMACS 4: algorithms for highly efficient, load-balanced, and scalable molecular simulation. J Chem Theor Comput 4:435–447. https://doi.org/10.1021/ct700301q
33. Möller D, Kling RC, Skultety M et al (2014) Functionally selective dopamine D2, D3 receptor partial agonists. J Med Chem 57:4861–4875. https://doi.org/10.1021/jm5004039
34. Goetz A, Lanig H, Gmeiner P, Clark T (2011) Molecular dynamics simulations of the effect of the G-protein and diffusible ligands on the β2-adrenergic receptor. J Molec Biol 414:611–623. https://doi.org/10.1016/j.jmb.2011.10.015
35. Schrodinger, LLC (2010) The PyMOL molecular graphics system, version 1.3r1. Schrodinger, LLC, New York
36. Pettersen EF, Goddard TD, Huang CC et al (2004) UCSF Chimera—a visualization system for exploratory research and analysis. J Comput Chem 25:1605–1612. https://doi.org/10.1002/jcc.20084